The Impact of 3-D Earth Structure on Far-Field Sea Level Following Interglacial West Antarctic Ice Sheet Collapse

Evelyn Powell[1**], Linda Pan[1], Mark Hoggard[1,2],
Konstantin Latychev[1], Natalya Gomez[3], Jacqueline Austermann[4] & Jerry X. Mitrovica[1]

1. Department of Earth and Planetary Sciences, Harvard University
2. Research School of Earth Sciences, Australian National University
3. Department of Earth and Planetary Sciences, McGill University
4. Department of Earth and Environmental Sciences, Columbia University

** *Corresponding author*.
Email: evelynpowell@g.harvard.edu
Maling address: Department of Earth and Planetary Sciences, 20 Oxford St., Cambridge, Ma 02138

This is the accepted manuscript. Link to publication:
https://doi.org/10.1016/j.quascirev.2021.107256.

Keywords: Interglacial(s); Sea-level change; Antarctica; Global; Data treatment, data analysis; Numerical modeling; Dynamics of lithosphere and mantle; Rheology

Abstract

Prior to inferring ice sheet stability from past interglacial sea-level records, these records must first be corrected for the contaminating effects of glacial isostatic adjustment (GIA). Typical GIA corrections, however, neglect variability in the signal that may be introduced by Earth's 3-D rheological structure. We predict sea-level changes due to a collapse of the West Antarctic Ice Sheet (WAIS) over an idealized 6 kyr-duration interglacial using four viscoelastic Earth models. Two of these are 3-D viscosity models inferred from seismic tomography fields. The third is a 1-D (depth varying) viscosity model equivalent to the spherically averaged "background" viscosity profile adopted in both 3-D Earth models. The fourth is a 1-D model that has a higher upper mantle viscosity but still falls within the class of models inferred from independent global GIA studies. We find that the discrepancy between 3-D and 1-D Earth model calculations of sea level in the far field of the melt zone is of order 0.3 m or less, with the 1-D Earth models producing higher sea level than the 3-D simulations. This value is 10% of the global mean sea-level (GMSL) rise associated with modeled ice sheet collapse by the end of the model interglacial (~3 m) and a similar fraction of far-field sea-level changes. However, the value is a significantly larger fraction (~60%) of the geographically variable (i.e., non-GMSL) component of the far-field sea-level signal due to GIA associated with modeled WAIS collapse (±0.5 m). Neglecting lateral variations in Earth structure in modeling the response to excess melting of WAIS during the interglacial compounds any error introduced by neglecting such structure in predictions of interglacial sea-level change driven by the preceding glacial cycle.

1. Introduction

The geologic record of sea level during past interglacials can provide insight into, and serve as a partial analogue for, the stability of ice sheets in our progressively warming world. The minimum extent of past ice sheets during such periods is primarily constrained by reconstructions of global mean sea level (GMSL). Although GMSL during Marine Isotope Stage (MIS) 11 (424-395 ka; the interglacial of longest duration over the past 500 kyr) is debated (Hearty et al., 1999; McMurtry et al., 2007), several studies indicate a peak value close to 10 m above present-day sea level (Raymo and Mitrovica, 2012; Chen et al., 2014). GMSL during MIS 5e (130-116 ka), also known as the Last Interglacial (LIG), remains debated and may have peaked 6-9 m (Kopp et al., 2009; Dutton and Lambeck, 2012; O'Leary et al., 2013; Clark et al., 2020) or 3-5 m (Dyer et al., 2021) above present-day sea level. These values suggest that, during these interglacials, there was substantial melting (i.e., retreat and thinning) of polar ice sheets beyond their present-day extent. During the LIG, excess melting of the Greenland Ice Sheet (GIS) is thought to have potentially contributed an additional ~1-4 m to GMSL (e.g., Otto-Bliesner et al., 2006; Helsen et al., 2013; NEEM, 2013; Stone et al., 2013), while the West Antarctic Ice Sheet (WAIS) may have contributed an additional ~3-4 m to GMSL (Bamber et al., 2009; Sutter et al., 2016; Pan et al., 2021). Outstanding questions concerning these interglacials include: which ice sheets contributed to the GMSL rise and by how much? And when and how quickly did these ice sheets collapse? Tackling these questions through careful interpretation of the geologic record is crucial to reducing uncertainties over ice sheet behavior during periods of sustained global warming.

Melting of ice sheets results in Earth deformational, gravitational and rotational perturbations in a process called glacial isostatic adjustment (GIA), and leads to a geographically variable sea-level response. Unfortunately, sea-level records only sample this signal at specific points in space and time, which makes accounting for the sources of complexity in this signal non-trivial. A common approach in geophysical analyses of interglacial sea-level records is to correct observations for the GIA signal associated with ice age cycles using a calculation in which GMSL across the interglacial period is assumed to be equal to the present-day value (e.g., Raymo and Mitrovica, 2012; Dutton and Lambeck, 2012; O'Leary et al., 2013; Chen et al., 2014; Polyak et al., 2018). Any residual sea-level signal is then generally attributed to "excess melt", i.e., melting of ice sheets and glaciers beyond their present-day state. Hay et al. (2014) showed that this approach, however, neglects any GIA effects arising due to the excess melt itself. For example, Dutton and Lambeck (2012) used MIS 5e coral records from Western Australia and the Seychelles and assumed that the residual signals at the two sites define lower and upper bounds on peak GMSL, respectively, and in doing so obtained their peak estimate of 5.5-9.0 m for the LIG. This value was subsequently revised to 5.5-7.5 m because GIA effects resulting from excess melting of either the GIS or WAIS would have produced a local sea-level rise at the Seychelles that is 15% larger than the corresponding GMSL change (Hay et al., 2014). Although several additional studies estimating GMSL have recognized that the excess melting signal would introduce geographic sea-level variability, and that there can be substantial differences between predictions that either instantaneously melt this excess ice or adopt a more physically realistic ice-sheet collapse, until recently they have generally assumed that any viscous response can be modeled using 1-D models of mantle viscosity (e.g., Chen et al., 2014; Hay et al., 2014).

In this article, we investigate the effect of lateral variations in mantle viscosity on predicted sea-level changes at far-field sites associated with excess ice mass flux from Antarctica during an interglacial. Hay et al. (2017) showed that accounting for 3-D Earth structure in modeling of WAIS collapse has a substantial impact on predictions of sea-level change close to the ice sheet, with the peak sea-level fall in the melt zone increasing by a factor of four at the end of a 1000-year collapse scenario due to 3-D viscous effects. This impact is perhaps unsurprising, given the significant lateral variations in mantle properties beneath WAIS, which involve upper mantle viscosities 2-3 orders of magnitude lower than cratonic areas commonly considered in GIA analyses (e.g., Kaufmann et al., 2005). Given that the near-field sea-level record is highly sensitive to both Earth structure and the exact geometry of local ice melting, it is generally considered a less useful constraint on GMSL than observations from the far field. Crawford et al. (2018) demonstrated that the sea-level response at a far-field site is most impacted by variations in mantle structure both beneath the site itself and within the region of the Earth beneath the ice melting zone, with additional sensitivity to structure along the path between these two locations.

We estimate the sea-level signal in the case of excess melting from WAIS using a time-varying model of ice sheet collapse (Gomez et al., 2015) in the presence of lateral variations in lithospheric thickness and mantle viscosity. We note that the impact of lateral variations in Earth structure on the GIA signal during an interglacial associated with ice mass flux in the prior glacial cycle, which we are not considering here, has recently been explored in detail by Austermann et al. (2021). Our goal in this study is to quantify the level of inaccuracy introduced by modeling the response to excess WAIS melting using only 1-D Earth models.

2. **Methods**

Our calculations of sea-level change are based on the gravitationally self-consistent theory of Kendall et al. (2005), as revised by Gomez et al. (2010). The theory incorporates the effect of shoreline migration, including water flux associated with changes in the perimeter of grounded, marine-based ice sheets. We adopt the ice age rotation theory of Mitrovica et al. (2005) to calculate the impact of perturbations in Earth's rotation on sea level. We use the general form of the sea-level theory valid for a Maxwell viscoelastic Earth model, in which mantle viscosity varies in three dimensions and the thickness of the lithosphere (treated as a region of infinite viscosity) varies laterally. All calculations are performed using the finite volume software described in detail in Latychev et al. (2005), and which has been subsequently altered to allow grid refinement in areas of interest (Gomez et al., 2018). The calculations require two inputs: the spatio-temporal history of grounded ice cover and the 3-D mantle viscosity structure. We describe each, in turn, below.

Figure 1 summarizes the grounded ice sheet history we adopt for WAIS collapse over an interglacial. The model is adapted from a coupled ice sheet-Earth-sea-level model simulation (Gomez et al., 2015; Pollard et al., 2017) in which marine-based sectors of WAIS retreat over 600 years through the marine ice sheet instability mechanism with applied climate warming (RCP8.5 emission scenario; Riahi et al., 2011). We have linearly scaled the timing by a factor of 10 so that the collapse takes place over 6000 years. Ice thickness at the end of the simulation is shown in Figure 1a. The rate of ice mass loss is muted for the first 1-2 kyr, but subsequently increases, with an approximately linear melt signal until 6 kyr, at which point 1.9×10^6 Gt of ice has melted. Using present-day bedrock topography, this maps into a change in the volume of ice above floatation equivalent to a GMSL change (i.e., the net volume of meltwater released outside the Antarctic divided by the area of the open ocean) of 2.68 m (Figure 1b, black box). (In the discussion below, we point out that a more accurate measure of GMSL change is 3.2 m.) The simulation ends with a collapse of most marine-based sectors of WAIS and a marginal increase in ice volume within the East Antarctic Ice Sheet (EAIS). No other ice sheets or glaciers are considered.

All Earth models adopt the 1-D (i.e., depth-varying) elastic and density structure from the seismically inferred Preliminary Reference Earth Model (PREM; Dziewonski and Anderson, 1981). We construct two 3-D Earth models as described in Pan et al. (2021). The globally averaged lithospheric thickness in both models is 96 km, and lateral variations in viscosity are superimposed on a background 1-D viscosity profile of 10^{20} Pa s in the upper mantle (shallower than 670 km) and 5×10^{21} Pa s in the lower mantle.

The first 3-D Earth model is based on the global seismic tomography model SEMUCB-WM1 (French and Romanowicz, 2015), with the tomography model of Schaeffer and Lebedev (2013), SL2013sv, in the top ~350 km of the upper mantle. Shear wave velocity anomalies are converted into lateral variations in temperature (see Richards et al., 2020, and Austermann et al., 2021, for details) and the thickness of the lithosphere is taken to be the depth of the 1175°C isotherm, yielding variations from 0 km along mid-ocean ridges up to ~350 km in the thickest portions of cratons (Richards et al., 2018; Hoggard et al., 2020; Figure 2a). The viscosity field varies laterally by three orders of magnitude in the upper mantle (Figure 2b). We label this model as $M3D_A$.

The second 3-D Earth model is described in Hay et al., (2017), a study which focused on the Antarctic near field. The lithospheric thickness variation is established by combining the models of An et al. (2015b) for the Antarctic plate and Conrad and Lithgow-Bertelloni (2006) elsewhere, yielding a peak lithospheric thickness of ~250 km (Figure 2c). The mantle viscosity is constructed by scaling a 3-D seismic velocity field generated by combining the global tomography model S40RTS (Ritsema et al., 2011) with the near-field Antarctic mantle tomography models of An et al. (2015a) for East Antarctica and Heeszel et al. (2016) for West Antarctica. The viscosity field of this model varies laterally by 5 orders of magnitude in the upper mantle (Figure 2d). This model will be referred to as $M3D_B$.

The difference in magnitude of viscosity variations between the two 3-D Earth models arises because the treatment of anelasticity in constructing $M3D_B$ from seismic velocity anomalies tends to overestimate the temperature effect in areas with high temperatures; we thus interpret it as an end-member model for the magnitude of lateral viscosity variations (see Austermann et al., 2021, for more details and a discussion of uncertainties in the viscosity conversion).

In addition, we consider results based on two 1-D Earth models. The first, termed $M1D_{p15}$, is identical to the spherically averaged profile of the 3-D Earth models. The second 1-D model, termed $M1D_{p55}$, is identical to the first with exception that the upper mantle viscosity is increased to 5×10^{20} Pa s. These models are within the class of models inferred in independent analyses of GIA data (Mitrovica and Forte, 2004; Lambeck et al., 2014).

3. **Results & Discussion**

The upper panels in Figure 3 show the total change in sea level across the full 6000-year simulation based on the 3-D Earth models $M3D_A$ and $M3D_B$. The general features in both are the same. In particular, relative to the GMSL change (3.2 m): (1) a major drawdown in sea level beneath WAIS (which is primarily obscured by the continental mask) and extends out to southern South America and New Zealand, which is driven by long-wavelength post-glacial elastic uplift and gravitational migration of water away from the collapsed ice sheet; (2) a sea-level rise immediately offshore of West Antarctica that punctuates zone (1) and reflects viscous crustal subsidence at the periphery of the ice sheet (i.e. peripheral bulge subsidence); (3) a so-called “quadrential” signature in the far field that is driven by rotational effects (Milne and Mitrovica, 1998). This third component occurs because melting from WAIS acts to reorient the south pole toward West Antarctica and the north pole toward Eurasia (Gomez et al., 2010), which drives sea-level rise in North America and the southern Indian Ocean and sea-level fall in the southwest Pacific Ocean and Eurasia. This signal is dwarfed by near-field effects in the southwest Pacific Ocean, while in Eurasia it is largely masked by continents, but it is evident in the eastern Mediterranean and Black Sea; and (4) also in the far field, a crustal tilting signal near continental shorelines (downward towards oceans) due to ocean loading, which is superimposed on the larger scale quadrential geometry. The well-developed peripheral subsidence signal (2) is a consequence of the low upper mantle viscosity in the vicinity of West Antarctica in both 3-D

Earth models; this region is more extensive in the case of the prediction based on Earth model $M3D_B$ relative to $M3D_A$ because the upper mantle viscosity is lower in the former (Figure 2). Note that the geographically variable (non-GMSL) component of the far-field signal due to GIA in Figures 3A and 3D peaks at ~±0.5 m.

The remaining frames in Figure 3 indicate that the impact of introducing 3-D Earth structure is greater in the case of predictions generated with Earth model $M3D_B$ than $M3D_A$. This reflects the significantly higher amplitude variability of mantle viscosity in the former relative to the latter (Figures 2b, d). In the near field of Antarctic ice loss (Figure 4), the difference between these 3-D model simulations and the 1-D predictions is lower in the case of the 1-D model $M1D_{p15}$ than $M1D_{p55}$, which would be expected given that model $M1D_{p15}$ has an upper mantle viscosity beneath WAIS that is closer to that of the 3-D models (Figures 2b,d). In the far field, the difference between predictions based on either of the 3-D models and the two 1-D models is similar regardless of whether one is considering model $M1D_{p15}$ or $M1D_{p55}$ (compare Figure 3b to 3c, or 3e to 3f). This suggests that the response to rotational effects and broad spatial scale water loading in the far field is not sensitive to the factor of five difference in upper mantle viscosity between the two 1-D models. A second interesting result is that the sign of the difference is mostly negative, i.e., the 1-D models are predicting a higher magnitude sea-level change than the 3-D models in almost the entire far-field region. We return to this point below.

In Figure 5, we show time series of the difference in sea-level predicted using 1-D and 3-D Earth models across the 6000-year simulations. The six sites have commonly been considered in LIG analyses (e.g., Barlow et al., 2018): San Salvador Island, Bahamas; Bristol Channel, UK; Bab-el-

Mandeb, Red Sea; La Digue Island, Seychelles; Cape Range, Western Australia; and Eyre Peninsula, Southern Australia. The locations of these six sites are shown in Figure 3. As one would expect on the basis of Figure 3, predictions generated using the Earth model $M3D_B$ show larger magnitude differences with the 1-D model simulations than the predictions based on $M3D_A$ (red versus blue lines), and with few exceptions, the 1-D models yield higher magnitude predictions of sea-level rise than the 3-D models. The difference between the solid and associated dashed line on each frame represents the difference in the response between the two 1-D models. This signal is generally small, although it is close to ~0.1 m for the Bristol Channel and Cape Range sites. This reflects a difference in the local response to ocean loading (i.e., continental levering; Mitrovica and Milne, 2002), with the lower upper mantle viscosity of model $M1D_{p15}$ yielding a greater tilting of the lithosphere.

In Figure 3, the neglect of 3-D Earth structure in modeling the far-field sea-level response to WAIS collapse peaks at ~0.3 m in the case of model $M3D_B$ and ~0.15 m in the case of $M3D_A$, with the 1-D models producing higher sea level than the 3-D models. These peak values are evident in Figure 5f. These bounds are ~10% and ~5%, respectively, of the GMSL rise of ~3 m associated with the ice history. However, the magnitude of the far-field signal introduced by including 3-D Earth structure (Figures 3b or 3e) is a much larger percentage of the geographically variable (i.e., non-GMSL) component of the total far-field sea-level signal that is due to GIA, which, from Figures 3a and 3d, reaches ±0.5 m, namely ~60% and ~30%, respectively.

To test the sensitivity of the results to the duration of the melt event, we repeated the simulations $M3D_B$ and $M3D_{p15}$ using a revised ice history in which the collapse timescale is reduced from 6 kyr to 3 kyr. We denote these simulations as $M3D_{B\text{-}3k}$ and $M1D_{p15\text{-}3k}$, respectively. Timeseries of the residual between these simulations at the six sites considered is shown in Figure 5 (black dotted line). These results indicate that the magnitude of the peak difference between the 3D and 1D runs is relatively insensitive to the timescale of collapse, and is generally achieved by the end of the collapse (compare black dotted line at 3 kyr with red solid line at 6 kyr).

To complete this section, we focus on understanding in more detail the origin of the signals in Figures 3 and 4.

Models of ice sheet evolution commonly quote a so-called change in "ice above floatation", which is the volume of ice that would leave the AIS after accounting for meltwater filling marine-based sectors that are exposed by retreating grounded ice. This quantity can then be expressed as a unit of GMSL by converting it to a volume of meltwater and evenly distributing the result across the open ocean, which we define as the ocean outside of Antarctica. As noted in the Methods section, our ice sheet model yields an ice above floatation change in GMSL of 2.68 m. However, this measure of GMSL change neglects the viscoelastic uplift of marine sectors, which acts to push additional meltwater out into the open ocean as a function of time (Gomez et al., 2010; Pan et al., 2021). Thus, a definition of GMSL that reflects the total meltwater released from the Antarctic must account for this additional mass flux across the sea-level simulation, which will depend upon the adopted Earth model. Figure 1b shows the GMSL change over the open ocean computed in this manner in the four simulations described above (solid and dashed lines). Due to the meltwater outflux process, GMSL is ~3.2 m at the culmination of the 3-D runs, which is ~0.5 m higher than the change in ice above floatation. In contrast, the meltwater outflux process is slower in the two 1-D models, contributing an additional 0.38 m in the case of model $M1D_{p15}$ and only 0.21 m in the higher viscosity model $M1D_{p55}$. We note that the rebound related outflux computed using the two 3-D Earth models (0.5 m, in units of GMSL) is approximately half the maximum value computed by Pan et al. (2021) using model $M3D_B$ and various WAIS collapse scenarios. The difference is due to the more extensive melting of marine-based sectors in those scenarios relative to Figure 1a.

If the 1-D Earth models are underestimating the flux of water out of exposed and rebounding sections of West Antarctica, why are these models overestimating the local sea-level rise in the far field, i.e., why do the far-field sections of the difference maps in Figure 3 (frames b, c, e, and f) and the time series in Figure 5 generally show negative values? The answer involves the dynamics of sea-level change in the 3-D and 1-D models outside Antarctica, and in particular the magnitude of the peripheral subsidence – and sea-level rise – immediately offshore West Antarctica (Figure 4). We computed the mean sea-level rise in the peripheral bulge within the longitude range 150°-360° E for each of the four simulations and obtained values of 5.15 m ($M3D_A$), 6.25 m ($M3D_B$), 4.17 m ($M1D_{p15}$), and 2.48 m ($M1D_{p55}$). The 3-D models yield greater subsidence of the peripheral bulge (sea-level rise) because the upper mantle viscosity offshore West Antarctica is significantly lower in these models relative to the 1-D models (Figures 2b,d). Peripheral subsidence draws water from the far field in a process termed ocean syphoning (Mitrovica and Milne, 2002), which contributes a sea-level fall in the far field. The difference in the magnitude of the peripheral subsidence and ocean syphoning between the 1-D and 3-D models overcompensates for the water outflux mechanism and bring the total sea-level rise in the far field predicted using the 1-D Earth models higher than the predictions based on the 3-D models. Of course, these effects are not geographically uniform and the variability in the far-field signals of Figures 3b, c, e, and f arises from other GIA effects, particularly ocean loading.

Pan et al. (2021) demonstrated that including the outflux of meltwater from exposed, marine-based sectors of WAIS was important for accurately predicting both GMSL rise associated with any WAIS collapse scenario and sea-level changes at specific geographic sites. As an example, the predicted sea-level rise at Bahamas at the end of the 3-D simulations is ~3.2 m (Figure 3a,d), equal to the GMSL computed (including the water outflux mechanism) for those simulations (Figure 1b), indicating that the signal from other GIA effects (peripheral subsidence, rotation, ocean loading, gravitational perturbations) combine to be close to zero at that site. As we noted above, the geographic variability evident in Figures 3a,d arises from a net signal from these processes, particularly the feedback of rotation on sea level.

In conclusion, our results show that modeling WAIS collapse with standard 1-D Earth models introduces two primary sources of inaccuracy in predictions of far-field sea-level change associated with dynamics within West Antarctica (water outflux) and outside of it (ocean syphoning due to peripheral bulge subsidence, ocean loading; Figure 3 and 4, bottom two rows). The net effect of these signals – that is, the error introduced by neglecting lateral variations in Earth structure in predicting the far-field sea-level response to WAIS collapse – is geographically variable, but, as we have noted, the magnitude of the error can represent a significant fraction of the geographically variable (non-GMSL) signal that is due to GIA.

Finally, we emphasize that this error will compound the additional error introduced by neglecting this structure in predictions of interglacial sea-level change driven by the preceding glacial cycle (Austermann et al., 2021).

Acknowledgements

This material is based upon work supported by the NSF Graduate Research Fellowship Grants DGE1144152 and DGE1745303 [E.M.P.], Fonds de Recherche du Québec–Nature et technologies [L.P.], Star-Friedman Challenge [L.P. and K.L.], NASA grant NNX17AE17G [J.X.M., E.M.P., and M.J.H.], NSF grant OCE-1702684 [J.X.M.], Geoscience Australia's Exploring for the Future research program [M.J.H.], Harvard University [E.M.P., L.P., M.J.H., K.L., and J.X.M.], Natural Sciences and Engineering Research Council of Canada [L.P. and N.G.], Canada Research Chairs program [N.G.], and NSF grant OCE 18-41888 [J.A.].

References

An, M., D. Wiens, Y. Zhao, M. Feng, A. A. Nyblade, M. Kanao, Y. Li, A. Maggi, and J.-J. Lévêque, S-velocity model and inferred Moho topography beneath the Antarctic Plate from Rayleigh waves, *J. Geophys. Res.*, 120, 359–383, 2015a.

An, M., D. Wiens, Y. Zhao, M. Feng, A. A. Nyblade, M. Kanao, Y. Li, A. Maggi, and J.-J. Lévêque, Temperature, lithosphere–asthenosphere boundary, and heat flux beneath the Antarctic Plate inferred from seismic velocities, *J. Geophys. Res.,* 120, 8720-8742, 2015b.

Austermann, J., M. Hoggard, K. Latychev, F. D. Richards, and J. X. Mitrovica, The effect of lateral variations in Earth structure on last interglacial sea level, *Geophys. J. Int.*, in press, 2021.

Bamber, J. L., R. E. M. Riva, L. L. A. Vermeersen, and A. M. LeBrocq, Reassessment of the potential sea level rise from a collapse of the West Antarctic Ice Sheet, *Science*, 324, 901–903, 2009.

Barlow, N. L. M., E. L. McClymont, P. L. Whitehouse, C. R. Stokes, S. S. R. Jamieson, S. A. Woodroffe, M. J. Bentley, et al., Lack of Evidence for a Substantial Sea-Level Fluctuation within the Last Interglacial, *Nat. Geoscience*, 11 (9): 627–34, 2018.

Chen, F., S. Friedman, C. G. Gertler, J. Looney, N. O'Connell, K. Sierks, and J. X. Mitrovica, Refining estimates of peak eustatic sea level during the MIS11 interglacial based on indicators from South Africa, *J. Clim.*, 27, 8740-8746, 2014.

Clark, P. U., F. He, N.R. Golledge, J. X. Mitrovica, A. Dutton, J. S. Hoffman, and S. Dendy, Oceanic forcing of penultimate deglacial and last interglacial sea-level rise. *Nature* **577**, 660–664, 2020.

Conrad, C. P., and C. Lithgow-Bertelloni, Influence of continental roots and asthenosphere on plate-mantle coupling, *Geophys. Res. Lett.*, 33, L05312, 2006.

Crawford, O., D. Al-Attar, J. Tromp, J. X. Mitrovica, J. Austermann, and H. Lau, Quantifying the sensitivity of post-glacial sea level change to laterally varying viscosity, *Geophys. J. Int.*, 214, 1324-1363, 2018.

Dutton, A., and K. Lambeck, Ice volume and sea level during the Last Interglacial, *Science*, 337, 216-219, 2012.

Dyer, B., J. Austermann, J. W. D'Andrea, R. C. Creel, M. R. Sandstrom, M. Cashman, A. Rovere, and M. E. Raymo, Sea-level trends across The Bahamas constrain peak last interglacial ice melt, *PNAS*, 118(33), 2021.

Dziewonski, A., and D. L. Anderson, Preliminary reference Earth model (PREM), *Phys. Earth Planet. Inter.*, 25, 297-356, 1981.

French, S., and B. Romanowicz, Broad plumes rooted at the base of the Earth's mantle beneath major hotspots, *Nature*, 525, 95–99, 2015.

Gomez, N., K. Latychev, and D. Pollard, A Coupled Ice Sheet–Sea Level Model Incorporating 3D Earth Structure: Variations in Antarctica during the Last Deglacial Retreat, *J. Clim.,* 31, 4041-4054, 2018.

Gomez, N., J. X. Mitrovica, M. E. Tamisiea, and P. U. Clark, A New Projection of Sea-Level Change in Response to Collapse of Marine Sectors of the Antarctic Ice Sheet, *Geophy. J. Int*, 180, 623-634, 2010.

Gomez, N., D. Pollard, and D. Holland, D., Sea-level feedback lowers projections of future Antarctic Ice-Sheet mass loss, *Nature Comm.*, 6, 8798-8805, 2015.

Hay, C. C., H. C. P. Lau, N. Gomez, J. Austermann, E. M. Powell, J. X. Mitrovica, K. Latychev, and D. A. Wiens, Sea-level fingerprints in a region of complex Earth structure: The case of WAIS, *J. Clim.*, 30, 1881-1892, 2017.

Hay, C. C., J. X. Mitrovica, N. Gomez, J. R. Creveling, J. Austermann, and R. Kopp, The sea-level fingerprints of ice sheet collapse during interglacial periods, *Quat. Sci. Rev.*, 87, 60-69, 2014.

Hearty, P. J., P. Kindler, H. Cheng, and R. L. A. Edwards, 120 m middle Pleistocene sea-level highstand (Bermuda and the Bahamas) due to partial collapse of Antarctic ice, *Geology*, 27, 375-378, 1999.

Heeszel, D. S., D. A. Wiens, S. Anandakrishnan, R. C. Aster, I. W. D. Dalziel, A. D. Huerta, A. A. Nyblade, T. J. Wilson, and J. P. Winberry, Upper mantle structure of the central and West Antarctica from array analysis of Rayleigh wave phase velocities, *J. Geophys. Res.*, 121, 1758-1775, 2016.

Helsen, W., W. Van De Berg, R. Van De Wal, M. Van Den Broeke, and J. Oerlemans, Coupled regional climate-ice-sheet simulation shows limited Greenland ice loss during the Eemian, *Climate of the Past*, 9, 1773-1788, 2013.

Hoggard, M. J., K. Czarnota, F. D. Richards, D. L. Huston, A. L. Jaques, and S. Ghelichkhan, Global distribution of sediment-hosted metals controlled by craton edge stability, *Nat. Geosci.,* 13, 504–510, 2020.

Kaufmann, G., P. Wu, and E. R.Ivins, Lateral viscosity variations beneath Antarctica and their implications on regional rebound motions and seismotectonics, *J. Geodyn.*, 39, 165-181, 2005.

Kendall, R., J. X. Mitrovica, and G. A. Milne, On Post Glacial Sea-Level: II. Numerical Formulation and Comparative Results on Spherically-Symmetric Earth Models, *Geophys. J. Int.,* 161, 679-706, 2005.

Kopp, R. E., F. J. Simons, J. X. Mitrovica, A. C. Maloof, and M. Oppenheimer, Probabilistic assessment of sea level during the last interglacial, *Nature*, 462, 863-867, 2009.

Lambeck, K., H. Rouby, A. Purcell, Y. Sun, and M. Sambridge, Sea level and global ice volumes from the Last Galcial Maximum to the Holocene, Proc. Nat. Acad. Sci., 111, 15,296-15,303, 2014.

Latychev, K., J. X. Mitrovica, J. Tromp, M. Tamisiea, D. Komatitsch, and C. C. Christara, Glacial Isostatic Adjustment on 3-D Earth Models: A Finite-Volume Formulation, *Geophys. J. Int.*, 161, 421-444, 2005.

McMurtry, G. M., D. R. Tappin, P. N. Sedwick, I. Wilkinson, J. Fietzke, and B. Sellwood, Elevated marine deposits in Bermuda record a late Quaternary megatsunami. *Sediment. Geol.*, 200, 155-165, 2007.

Milne, G. A., and J. X. Mitrovica, Post-glacial sea level on a rotating Earth, *Geophys. J. Int.*, 133, 1-19, 1998.

Mitrovica, J. X., and A. M. Forte, A new inference of mantle viscosity based upon a joint inversion of convection and glacial isostatic adjustment data, *Earth Planet. Sci. Lett.,* 225, 177-189, 2004.

Mitrovica, J.X., and G. A. Milne, On the origin of Late Holocene highstands within equatorial ocean basins, *Quat. Sci. Rev.*, 21, 2179-2190, 2002.

Mitrovica, J. X., J. Wahr, I. Matsuyama, and A. Paulson, The Rotational Stability of an Ice-Age Earth, *Geophys. J. Int.,* 161, 491-506, 2005.

NEEM community members, Eemian interglacial reconstructed from a Greenland folded ice core, *Nature*, 493, 489–494, 2013.

O'Leary, M. J., P. J. Hearty, W. G. Thompson, M. E. Raymo, J. X. Mitrovica, and J. M. Webster, Ice sheet collapse following a prolonged period of stable sea level during the last interglacial, *Nat. Geosci.*, 6, 706-800, 2013.

Otto-Bliesner, B. L., S. J. Marsha, J. T. Overpeck, G. H. Miller, A. X. Hu, and CAPE, Simulating Arctic climate warmth and icefield retreat in the last interglaciation, *Science*, 311, 1751– 1753, 2006.

Pan L., E. M. Powell, K. Latychev, J. X. Mitrovica, J. R. Creveling, N. Gomez, M. J. Hoggard, and P. U. Clark, Rapid postglacial rebound amplifies sea level rise following West Antarctic Ice Sheet collapse, *Science Adv.*, 7, eabf7787, 2021.

Pollard, D., N. Gomez, and R. DeConto, Variations of the Antarctic Ice Sheet in a coupled ice sheet–Earth–sea level model: Sensitivity to viscoelastic Earth properties. *J. Geophys. Res. Earth Surf.*, 122, 2124–2138, 2017.

Polyak, V. J., B. P. Onac, J. J. Fornós, C. C. Hay, Y. Asmerom, J. A. Dorale, J. Ginés, P. Tuccimei, and A. Ginés, A highly resolved record of relative sea level in the western Mediterranean Sea during the last interglacial period, *Nat. Geosci.*, 11, 860-864, 2018

Raymo, M., and J. X. Mitrovica, Collapse of Polar Ice Sheets During the Stage 11 Interglacial, *Nature*, 483, 453-456, 2012.

Riahi, K., S. Rao, V. Krey, C. Cho, V. Chirkov, G. Fischer, G. Kindermann, N. Nakicenovic, and P. Rafaj, RCP8.5 – A scenario of comparatively high greenhouse gas emissions, *Clim. Change*, 109, 33-57, 2011.

Richards, F. D., M. J. Hoggard, L. R. Cowton, and N. White, Reassessing the thermal structure of oceanic lithosphere with revised global inventories of basement depths and heat flow measurements, *J. Geophys. Res. Solid Earth*, 123, 9136–9161, 2018.

Richards, F. D., M. J. Hoggard, N. White, and S. Ghelichkhan, Exploring the relationship between upper mantle structure and short wavelength dynamic topography using calibrated anelasticity parameterizations, *J. Geophys. Res. Solid Earth*, 125, e2019JB019062, 2020.

Ritsema, J., A. Deuss, H. van Heijst, H., and J. Woodhouse, S40RTS: a degree-40 shear-velocity model for the mantle from new Rayleigh wave dispersion, teleseismic traveltime and normal-mode splitting function measurements, *Geophys. J. Int.*, 184, 1223-1236, 2011.

Schaeffer, A. J., and S. Lebedev, Global shear speed structure of the upper mantle and transition zone, *Geophys. J. Int.*, 194, 417-449, 2013.

Stone, E. J., D. J. Lunt, J. D. Annan, and J. C. Hargreaves, Quantification of the Greenland ice sheet contribution to Last Interglacial sea level rise, *Clim. Past*, 9, 621-639, 2013.

Sutter, J., P. Gierz, K. Grosfeld, M. Thoma, and G. Lohmann, Ocean temperature thresholds for Last Interglacial West Antarctic collapse, *Geophys. Res. Lett.*, 43, 2675-2682, 2016.

Figures

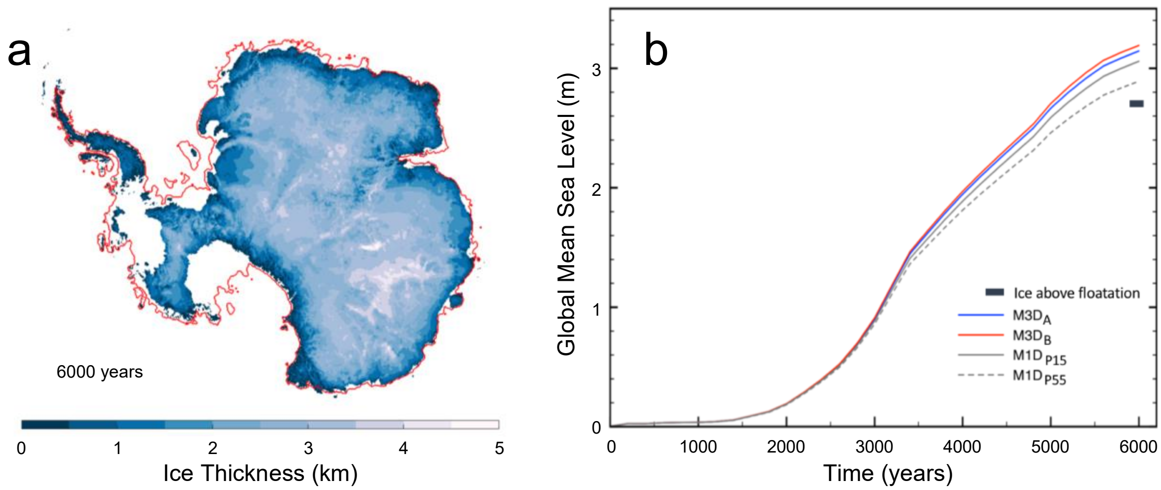

Figure 1. Ice History. (a) Thickness of the Antarctic Ice Sheet (km) at the end of the 6000-year ice melting scenario used in the calculations. The red contour shows the extent of the ice sheet at the start of the simulation. (b) Calculations of global mean sea-level change relative to present-day (see text for definition), distinguished on the basis of the adopted Earth model (as labeled). The small, black rectangle is the associated ice above floatation (2.68 m) of the ice history.

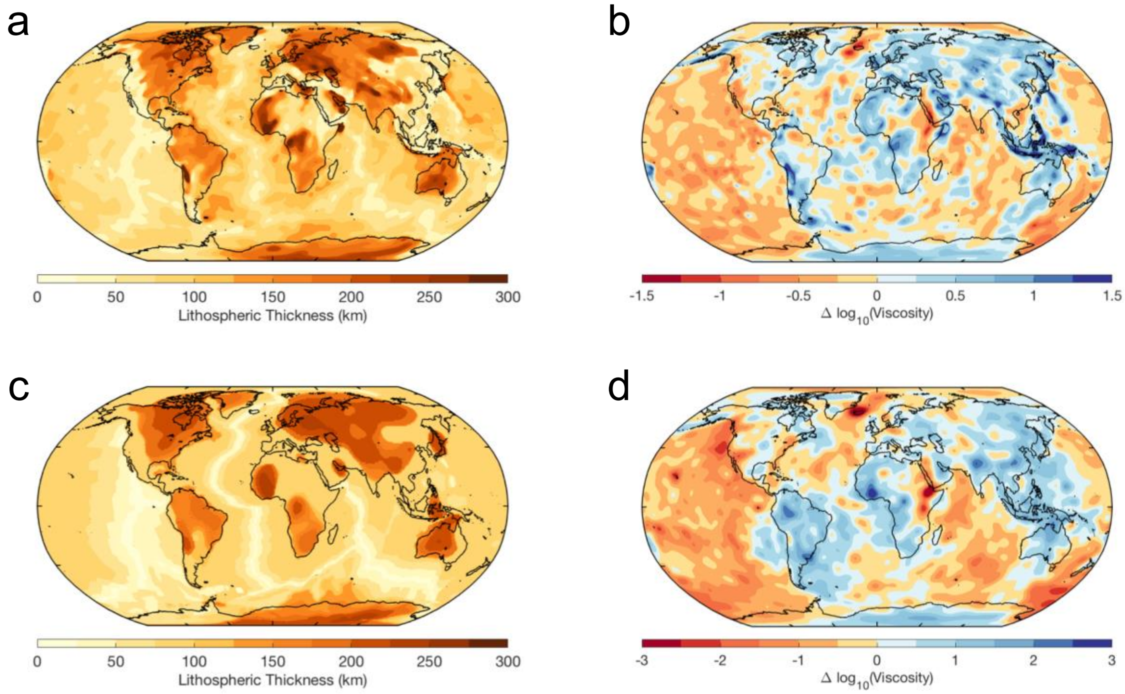

Figure 2. Viscoelastic Earth Models. (a) Lithospheric thickness in the 3-D viscoelastic Earth model $M3D_A$. (b) Average upper mantle viscosity variations for that model, depicted as the logarithm of depth-averaged upper mantle viscosity variations relative to a background value of 10^{20} Pa s, ($\log(\nu_{3D}/\nu_{1D})$). (c-d) As in (a-b), but for Earth model $M3D_B$. Note the difference in scale between (b) and (d).

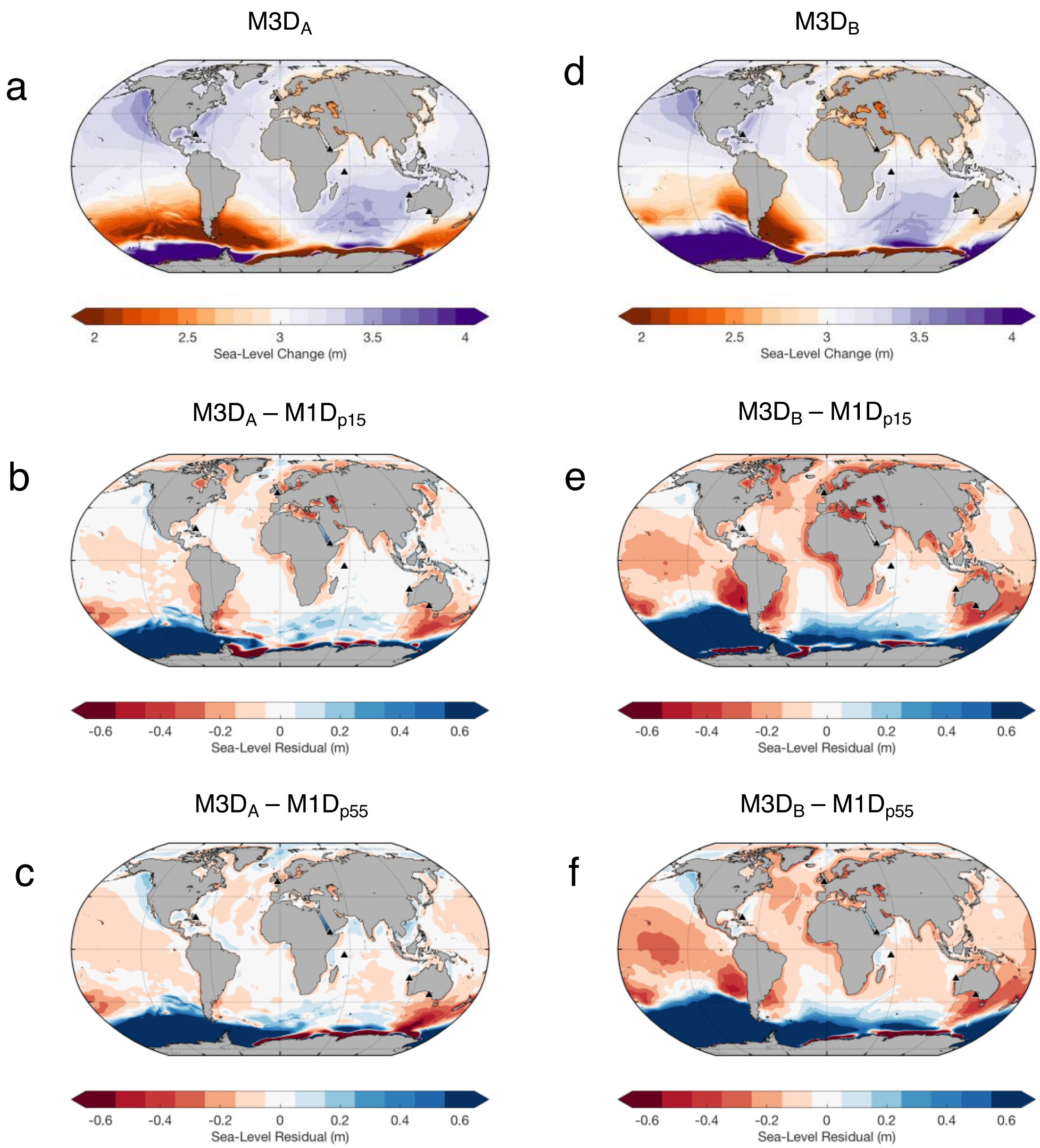

Figure 3. Sea-Level Predictions. (a) Sea-level change at the end of the 6000-year simulation predicted using the ice history summarized in Figure 1 and the viscoelastic Earth model $M3D_A$. (b,c) The difference in the sea-level prediction for $M3D_A$ and predictions based on the 1-D Earth models $M1D_{p15}$ and $M1D_{p55}$, respectively (i.e., 3-D prediction minus 1-D prediction). (d-f) Analogous to (a-c) with the exception that the 3-D Earth model $M3D_B$ is adopted. The black triangles in each frame denote locations of six sites considered in the sea-level time series of Figure 5.

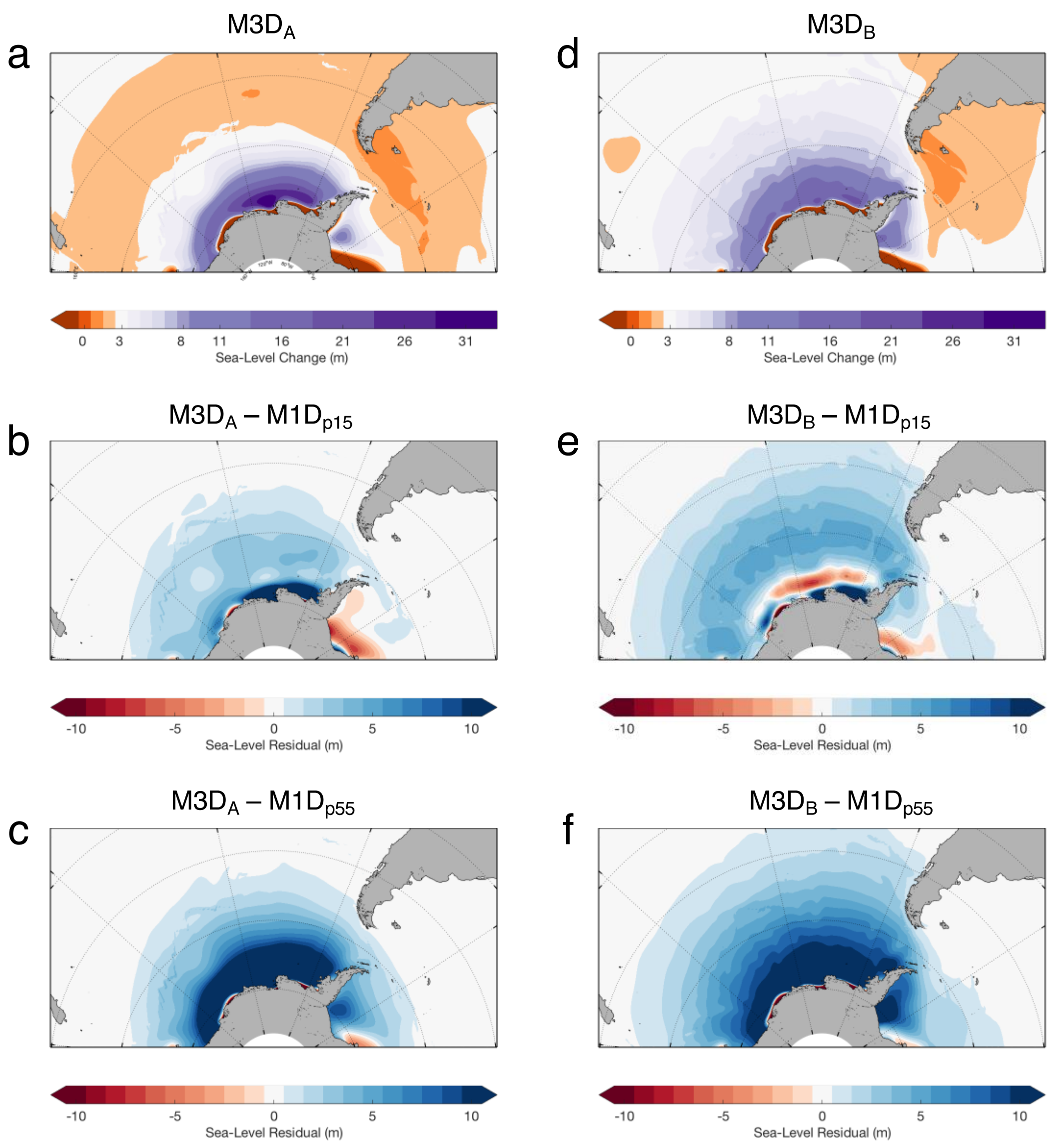

Figure 4. WAIS Near-Field Sea-Level Predictions. (a) Sea-level change in the near field of WAIS at 6000 years predicted using the viscoelastic Earth model $M3D_A$. (b,c) The difference in the near-field sea-level prediction for $M3D_A$ and predictions based on the 1-D Earth models $M1D_{p15}$ and $M1D_{p55}$, respectively (i.e., 3-D prediction minus 1-D prediction). (d-f) Analogous to (a-c) with the exception that the 3-D Earth model $M3D_B$ is adopted.

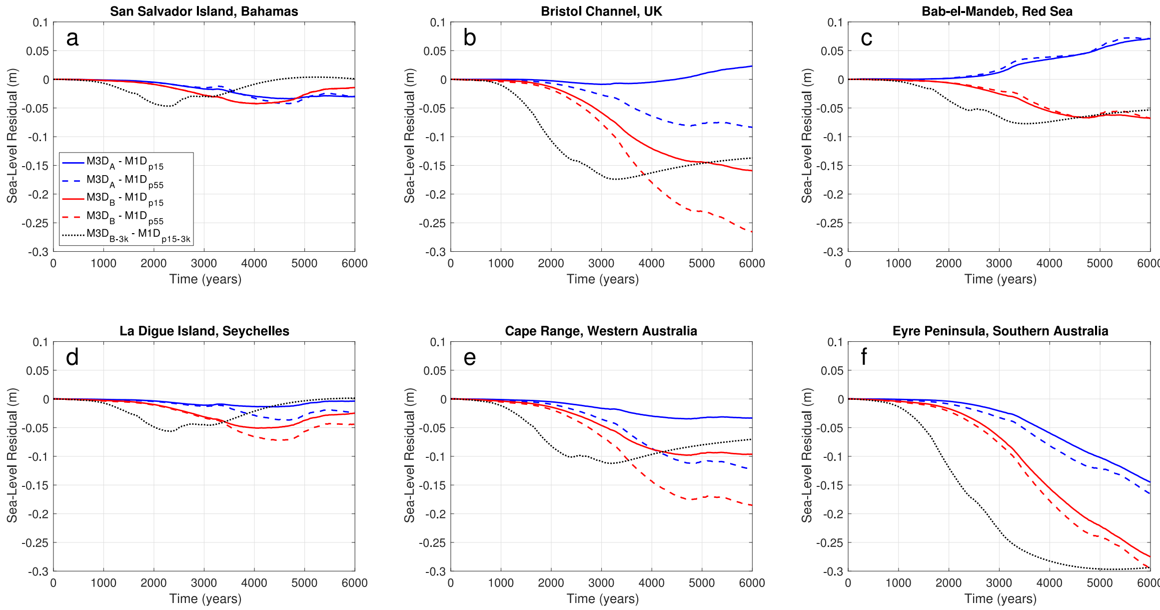

Figure 5. Time Series of Residual Sea-Level Predictions. Difference in sea-level change predicted using 3-D and 1-D Earth models across the 6000-year simulation at the six sites shown in Figure 3: (a) San Salvador Island, Bahamas (24.01 N, -74.52 E); (b) Bristol Channel, UK (55.51 N, -2.74 E); (c) Bab-el-Mandeb, Red Sea (12.60 N, 43.33 E); (d) La Digue, Seychelles (4.68 S, 55.50 E); (e) Cape Range, West Australia (22.12 S, 113.89 E); (f) Eyre Peninsula, South Australia (34.50 S, 136.00 E).